Fragmentation of gold projectiles with energies of 200–980 MeV/nucleon. II. Multiplicity distributions and correlations

C. Lewenkopf,[1] J. Dreute,[2] A. Abul-Magd,[1] J. Aichelin,[1]
W. Heinrich,[2] J. Hüfner,[1] G. Rusch,[2] and B. Wiegel[2]
[1]*Institut für Theoretische Physik, Universität Heidelberg, 6900 Heidelberg, Germany and Max-Planck-Institut für Kernphysik, 6900 Heidelberg, Germany*
[2]*Fachbereich Physik, Universität GH Siegen, 5900 Siegen, Germany*
(Received 21 February 1991)

We analyze the largest set of fragment coincidence data at present available, that of the preceding paper. This set contains all projectile fragments $6 \leq Z \leq 65$ produced in 6610 events of Au+Ag and Au+CR-39. We introduce a classification scheme based on the number of heavy fragments in order to define multifragmentation, spallation, and fission events. The multiplicity distribution $P(m_Z)$ is Poissonian, and the mean multiplicity as a function of Z can be described either by a power law or by an exponential. The slopes are independent of the projectile energy but depend on the target. While all investigated observables indicate that the multifragmentation in the case of a Ag target is a statistical process, we observe angular correlations in the case of the CR-39 target which indicate that probably the geometry and not the excitation energy is essential. Charge correlations are strong and only partially understood as yet. We find no positive sign for a liquid gas phase transition.

I. INTRODUCTION

In collisions with a proton or a heavy ion a heavy target nucleus can fragment into one or several nuclei $Z > 2$, plus nucleons and α particles. Depending on the number of light and heavy nuclear fragments, one distinguishes multifragmentation (no heavy and several light fragments), spallation (one heavy and up to a few light fragments) and fission (two heavy fragments) [1]. The boundary between light and heavy fragments lies around $Z = 20$ (see below). Nuclei with charge $Z = 1, 2$ have to be treated separately because they may come from quite different sources. Whereas fission and spallation are reasonably well understood, multifragmentation is to a large extent unknown land. A detailed investigation of the fragmentation processes requires the *coincident* measurement of the fragments formed in a heavy-ion collision. Only few experiments have been performed so far [2–4], which measure more than the inclusive mass yield of fragments. Most of them are emulsion experiments [3,4] with inverse kinematics. They suffer from the drawbacks of low statistics and the uncertainty of the target (protons to silver nuclei). Due to the deceleration of the nuclei in the emulsion each event takes place at different effective beam energy and one obtains the whole energy dependence of the process. In view of the very limited number of events this is unwanted and enforces an averaging over wide beam energy bins in the analysis. According to these experiments multifragmentation occurs already at a beam energy of 20 MeV/nucleon [4–7]. Below 100 MeV/nucleon multifragmentation is a rare process, the multiplicity of fragments in one event is low, and multifragmentation seems to occur in central collisions. The counter experiments [5–7] suffer from experimental threshold effects that leave most of the fragments (especially the heavy remnants) undetected. Thus in addition to the total mass yield only two fragment coincidences have been recorded. Emulsion experiments have shown [4] that in central collisions the number of fragments increases fast with energy (by a factor of 2 between 25 MeV/nucleon and 100 MeV/nucleon). Above 100 MeV/nucleon only two counter experiments have been reported [2,8–10]. Warwick and Wieman [2] have measured the α and Ne induced reaction with an Au target at several energies between 250 MeV/nucleon and 2.1 GeV/nucleon. This experiment in which the counters cover only a small fraction of 4π has produced the first coincidence fragment yields and has established—by measuring the associated multiplicity of fast particles—that multifragmentation occurs mainly in central collisions. Furthermore, the double differential cross section is measured and contradicts the assumption of emission from an equilibrated source. The plastic ball group [8–10] has observed multifragmentation in Au+Au collisions at 200 MeV/nucleon in a 4π device. However, only the projectilelike fragments with $3 \leq Z \leq 6$ have been recorded. This experiment has established that fragments show an even stronger flow than protons. Though rarely, events with up to 12 fragments with $3 \leq Z \leq 6$ have been recorded.

Due to the lack of coincidence data the theoretical investigations have concentrated on the explanation of the mass yield curve. For $Z \lesssim 20$ this curve is often parametrized by a power-law dependence $\sigma(Z) \sim Z^{-\tau}$ where the coefficient τ is around $\tau \approx 2.3$ and almost independent of projectile, target, and energy. As pointed out by Fisher [11] and later by Panagiotou [12] this form of the mass-yield curve as well as the value of $\tau = 2.3$ is expected when the transition between the liquid and gaseous phases occurs in nuclear matter. The perspective, to

study this phase-transition experimentally, has created a lot of excitement. However, later investigations have shown that a power-law form of the fragment yields is also seen in nonthermal processes like the distribution of the size of astroids [13]. Also a variety of different models, which assume quite different mechanisms for multifragmentation, predict this power-law dependence of the mass yield. Thus it certainly is not an unambiguous signal for the above-mentioned phase transition.

Only few of these models are able to predict more than the mass yield of the fragments. They fall into four classes: thermal models, percolation and statistical models, phenomenological models, and molecular dynamics calculations. The thermal models, either assuming instantaneous [14–17] or sequential decay [18–21] are mostly applied to p-induced reactions where all experimental observables have a form expected from a system in global equilibrium. They have problems with the experimental observation that both the double differential cross section and the isotopic distribution look thermal but the temperatures are quite different, 15 and 3 MeV, respectively. Percolation models [22–26] treat multifragmentation like percolation of a lattice and study the mass yield for different bond-breaking probabilities that may depend on the location in the lattice to simulate the geometry of the reaction. The phenomenological models [27–29], restricted to heavy-ion-induced reactions, yield quite reasonable triple differential cross sections $d^3\sigma/d\Omega\, dE\, dZ$ and are able to give reasons for the different apparent temperatures mentioned above. Recently it has become possible to simulate heavy-ion reactions on an event by event basis. In these so-called quantum molecular dynamical calculations [30–34] the trajectories of all nucleons are followed from the initial state prior to the reaction up to the final state where singles and fragments are recorded in the detectors. These calculations yield a remarkably good agreement with experimental multifragmentation results but are very computer-time consuming. Therefore the process that causes the fragmentation in these calculations up to now has only been revealed for asymmetric collisions at 84 MeV/nucleon [32] and 1 GeV/nucleon [30]. There are also classical molecular dynamics calculations [35] and a few hybrid models that try to simulate the dynamics in the entrance channel either by applying cascade calculations [36], mean-field calculations [37], or by assuming a certain momentum distribution [25]. In these models, at a certain point in time, the fragments are formed by a more or less phenomenological description and reflect some of the dynamics of the entrance channel.

The aim of this paper is an analysis of results from an experiment [38] that has measured all fragments with $6 \le Z \le 65$ on an event-by-event basis. The 6610 events contain data for Au+Ag and Au+CR-39 at 200 to 980 MeV/nucleon, where CR-39 denotes the plastic detector foil with the composition $C_{12}H_{18}O_7$. For each reaction all fragments with $6 \le Z \le 65$ are identified and their angles in the plane perpendicular to the beam direction are measured. The detection efficiency for smaller and larger fragments is below 1. In this paper we will analyze the information contained in the distribution of fragment sizes and in the kinematical variables. In Sec. II we will investigate multiplicity distributions and correlations under different constraints. Section III describes the charge and the angular correlations and studies the dependence on total multiplicity, energy, and target mass. In Sec. IV we discuss the conjecture of a phase transition and draw our conclusions.

II. MULTIPLICITY DISTRIBUTIONS AND CORRELATIONS OF LIGHT FRAGMENTS

A. Multifragmentation

What is multifragmentation? There is no commonly accepted definition for this process. We find it convenient to introduce a separation between light (L) and heavy (H) fragments. The three processes spallation, fission, and multifragmentation may then be distinguished by the multiplicity M_H of heavy fragments, $M_H=1$ for spallation, $M_H=2$ for fission, and $M_H=0$ for multifragmentation. Where is the boundary between heavy and light fragments? To answer this question we have investigated various observables and their systematics. The most convincing representation has been a plot of the charge yield $Y(Z)$ of fragments with a given Z for events with total multiplicity $M=1$ (Fig. 1). One clearly observes two domains where in each an exponential law holds. The transition appears between $Z=15$ and 25. The behavior of the charge yields with total multiplicities $M=2$ and $M=3$ [38] also points to $Z \approx 20$ as a boundary separating different reaction mechanisms. In order to avoid a possible confusion as to the nature of the fragments in the transition region, we will define heavy fragments by $Z_H \ge 25$ and light fragments by $Z_L \le 15$. As described in [38], for reasons of detection efficiency the charge of the light fragments is limited also from below by $Z_L \ge 6$. With this definition spallation and fission

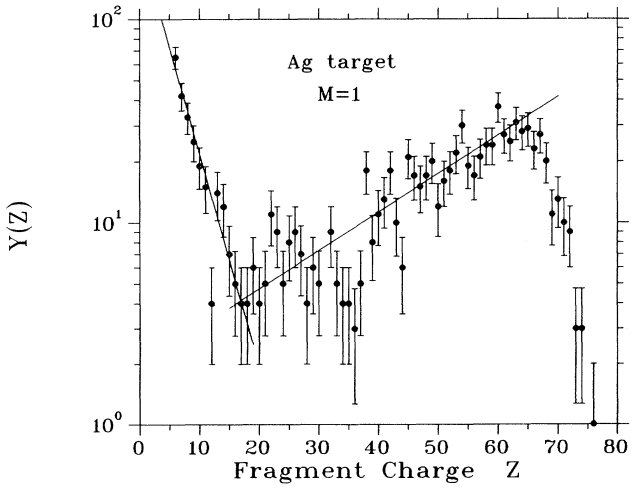

FIG. 1. Experimental charge yield $Y(Z)$ for multiplicity $M=1$ events as a function of the charge Z for the Ag target. The lines are exponential fits in the regions $6 \le Z \le 15$ and $30 \le Z \le 65$, respectively.

events are unambiguously characterized by $M_H=1$ and $M_H=2$, respectively. For multifragmentation, $M_H=0$, we select only those events where all fragments are light, $Z\leq 15$. Therefore all events containing a fragment with $16\leq Z\leq 24$ as the heaviest fragment are excluded from the analysis presented in this chapter.

We admit that the classification scheme and in particular the chosen value $Z\simeq 20$ as the boundary between light and heavy fragments contains a certain degree of arbitrariness. Certain conclusions in this chapter may be influenced by this choice.

B. Poisson test

Multifragmentation seems to be a statistical process, at least according to the general theoretical belief. How can this hypothesis be quantified? We call m_Z the number of projectile fragments with charge Z observed in one event and define by $P_L(m_6,\ldots,m_{15})$ the probability distribution for events with multiplicities $m_6,\ldots,m_{15}$. The limited statistics of our experimental sample does not permit the determination of the complete function P_L. Rather we investigate certain integrated observables, like moments of P_L or the distribution $P(M_L)$ of light particles. Be M_L the multiplicity of light fragments of an event

$$M_L=\sum_{Z=6}^{15} m_Z \ , \tag{1}$$

then the probability distribution $P(M_L)$ can be calculated from P_L to be

$$P(M_L)=\sum_{\{m_6,\ldots,m_{15}\}} P_L(m_6,\ldots,m_Z,\ldots,m_{15}) \times\delta\left[M_L-\sum_{Z=6}^{15} m_Z\right] . \tag{2}$$

Figure 2 shows the multiplicity distributions $P(M_L)$ for the Ag target data. Within error bars and excluding the value at $M_L=0$ the data are consistent with a Poisson distribution. The events with $M_L=0$ pose a serious problem. According to detection efficiencies an event with $M_L=0$ is one in which the Au nucleus fragments into "invisible" charges with $Z<6$ only. The measured number of these events in our sample is $N(M_L=0)=637$ for an Ag target. This experimental value, shown in Fig. 2 as a box, does not obey the Poisson systematics. Rather the value predicted for $M_L=0$ from the Poissionian that fits for $M_L>0$ is a factor of about 2 below the data point. This discrepancy may have at least two explanations: (i) The multiplicity distribution is not a Poissonian. (ii) The events with $M_L=0$ are a mixture of multifragmentation events (with at least one fragment having $3\leq Z\leq 5$ and presumably obeying Poisson statistics) and events in which only hydrogen and helium nuclei are produced. The latter ones cannot obey Poisson statistics for reasons of charge conservation. In this paper we favor the second alternative. We determine the fraction of multifragmentation events contained in $M_L=0$ events by extrapolating the Poisson fit to $M_L=0$. In this way we obtain a value $N_L(0,0,\ldots,0)$ of events that have no visible fragment.

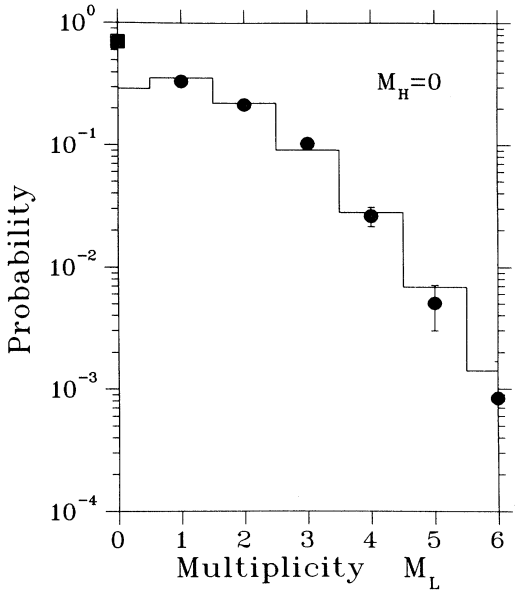

FIG. 2. Multiplicity distribution of multifragmentation ($M_H=0$) events for the Ag target. The experimental points for $M_L>0$ (circles) are fitted by a Poissonian with mean value $\langle M_L\rangle=1.18$. The situation for $M_L=0$ is discussed in the text.

The probability distribution P_L is defined by

$$P_L(m_6,\ldots,m_{15})=\frac{N_L(m_6,\ldots,m_{15})}{N} \ , \tag{3}$$

where $N_L(m_6,\ldots,m_{15})$ is the number of events with multiplicities m_Z for charge Z. The total number N of events includes the extrapolated value $N_L(0,0,\ldots,0)$.

We define the moments of P_L by

$$\langle m_Z^n\rangle=\sum_{\{m_6,\ldots,m_{15}\}} m_Z^n P_L(m_6,\ldots,m_{15}) \ ,$$
$$\langle m_{Z_1}^{n_1} m_{Z_2}^{n_2}\rangle=\sum_{\{m_6,\ldots,m_{15}\}} m_{Z_1}^{n_1} m_{Z_2}^{n_2} P_L(m_6,\ldots,m_{15}) \tag{4}$$

and introduce the correlation function $C(Z_1,Z_2)$ via

$$C(Z_1,Z_2)=\frac{\langle m_{Z_1}\cdot m_{Z_2}\rangle-\langle m_{Z_1}\rangle\langle m_{Z_2}\rangle}{\sqrt{\langle m_{Z_1}\rangle\langle m_{Z_2}\rangle}} \ . \tag{5}$$

Neglecting charge conservation and assuming that the fragment charges are statistically uncorrelated, we expect

$$C(Z_1,Z_2)=0, \quad \text{for } Z_1\neq Z_2 \ . \tag{6}$$

Charge conservation may safely be neglected for multifragmentation events since the mean observed charge of an event is small compared to the projectile charge. The value of the correlation function for $Z_1=Z_2$ depends on the underlying multiplicity distribution. We find

$$C(Z,Z)=\frac{\langle m_Z^2\rangle-\langle m_Z\rangle^2}{\langle m_Z\rangle}=\begin{cases}1 & \text{(Poissonian)}\\ 1+\langle m_Z\rangle & \text{(Exponential)}\end{cases}. \tag{7}$$

In order to distinguish between different distributions it is convenient to extract the quantity

$$Q(Z_1,Z_2)=[C(Z_1,Z_2)-\delta_{Z_1,Z_2}]/\sqrt{\langle m_{Z_1}\rangle\langle m_{Z_2}\rangle} \tag{8}$$

from the data. The quantity $Q(Z,Z)$ is zero for a Poissonian distribution and equals one for an exponential. The values of $Q(Z_1,Z_2)$ derived from the experimental data for the multifragmentation events with the Ag target are contained in Table I. They are all considerably smaller than 1 and within statistics indicate that indeed the correlation function satisfies

$$C(Z_1,Z_2)=\delta_{Z_1,Z_2}\quad (M_H=0)\ ; \tag{9}$$

i.e., (i) fragments with different charges $Z_1\neq Z_2$ occur uncorrelatedly, and (ii) the multiplicity distribution of fragments with charge Z is a Poissonian.

From Eq. (9) we can give an explicit expression for the probability distribution $P_L(m_6,\ldots,m_Z,\ldots,m_{15})$ to find light fragments with multiplicities m_Z:

$$P_L(m_6,\ldots,m_{15})=\prod_{Z=6}^{15}\frac{\langle m_Z\rangle^{m_Z}}{m_Z!}e^{-\langle m_Z\rangle}\ . \tag{10}$$

It is a product of Poisson distributions $P_Z(m_Z)$ with mean values $\langle m_Z\rangle$. These mean values $\langle m_Z\rangle$ are parameters yet to be determined.

If one inserts the expression Eq. (10) into Eq. (2) for $P(M_L)$, one obtains a Poissonian, since the folding of Poissonians leads to a Poissonian. This result confirms the findings of Fig. 2.

C. Multiplicity triggers

We investigate averages of the form $\langle m_Z\rangle_{M_L}$, where the averaging is taken over all multifragmentation events with a fixed multiplicity M_L of light fragments. These averages can be calculated from the probability distribution

$$P_L(m_6,\ldots,m_{15};M_L)=P_L(m_6,\ldots,m_Z,\ldots,m_{15})\times\delta\left[M_L-\sum_{Z=6}^{15}m_Z\right]. \tag{11}$$

One finds for the Poissonian ansatz Eq. (10)

$$\langle m_Z\rangle_{M_L}=\frac{M_L}{\langle M_L\rangle}\langle m_Z\rangle\ ,\qquad \frac{\langle m_Z^2\rangle_{M_L}-\langle m_Z\rangle_{M_L}^2}{\langle m_Z\rangle_{M_L}}=1-\langle m_Z\rangle\frac{M_L}{\langle M_L\rangle}\ . \tag{12}$$

Because of the additional constraint in Eq. (11), the distribution of the multiplicities m_Z for given M_L is no more a Poissonian. Yet the mean multiplicity $\langle m_Z\rangle_{M_L}$ has a very simple relation to the unconditional multiplicity $\langle m_Z\rangle$: it grows linearly with M_L. The data points for $\langle m_Z\rangle_{M_L}$ are displayed in Fig. 3 as squares. The line is obtained by a two-parameter fit of the form $ae^{-\mu Z}$. The slopes μ do not depend on M_L. The values a are compatible with $M_L/\langle M_L\rangle$; these values are marked by the diamonds in each figure. The statistics of the experimental events do not permit a significant test of the prediction for the dispersion in Eq. (12).

D. The Z dependence of $\langle m_Z\rangle$

In this section we discuss the Z dependence of $\langle m_Z\rangle$, the only open parameters in P_L, Eq. (10). Figures 4 and 5 show $\langle m_Z\rangle$ as a function of Z for $6\le Z\le 15$. Figure 4 shows the dependence of $\langle m_Z\rangle$ vs Z for the fragmentation of Au on Ag for various energy bins for the projectile. The solid lines are one-parameter fits of the form $e^{-\mu Z}$. The values of μ are independent of energy within the error bars. A two-parameter fit of the form $ae^{-\mu Z}$ does not yield a better reduced χ^2 value, therefore we conclude $a=1$. While in Fig. 4 $\ln\langle m_Z\rangle$ is displayed vs Z, we show in Fig. 5 $\ln\langle m_Z\rangle$ vs $\ln Z$. A straight line in a semilogarithmic representation indicates an exponential behavior $\langle m_Z\rangle=ae^{-\mu Z}$, whereas a power-law behavior $\langle m_Z\rangle=bZ^{-\tau}$ leads to a straight line in a double logarithmic representation. Due to the limited size of the Z interval we find it impossible to distinguish among the two functional forms. However, we would like to mention that a power-law fit of the data requires two adjustable parameters (b,τ), while our exponential fit $\langle m_Z\rangle=e^{-\mu Z}$ requires just one.

We summarize our observations: (i) The multiplicity m_Z of fragment Z obeys a Poisson distribution with mean value $\langle m_Z\rangle$. (ii) The Z dependence of $\langle m_Z\rangle$ can equally well be described by a power law and an exponential behavior $\langle m_Z\rangle=e^{-\mu Z}$. (iii) The slope parameter μ is independent of energy (above 200 MeV/nucleon), but de-

TABLE I. The correlation matrix $Q(Z_1,Z_2)$ multiplied by 100 [Eq. (8)] binned in intervals of two charges for $M_H=0$. On the left-hand side we display the matrix, on the right-hand side the error $\sigma_Q(Z_1,Z_2)$.

		Z_1							Z_1				
		6	8	10	12	14			6	8	10	12	14
	6	−8.5						6	14.5				
	8	−5.2	13.9					8	9.8	30.6			
Z_2	10	−14.9	−1.2	−11.8			Z_2	10	11.4	15.6	55.7		
	12	−4.9	1.0	38.6	30.5			12	13.6	17.5	26.4	80.4	
	14	17.4	−21.0	−51.8	2.9	−32.6		14	18.4	17.4	16.2	28.0	118.4

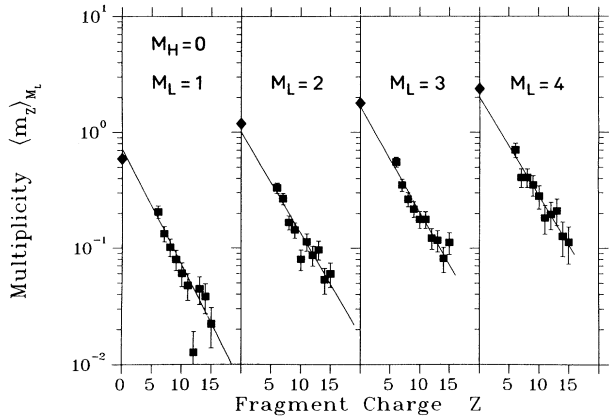

FIG. 3. Experimental mean multiplicity $\langle m_Z \rangle$ vs Z of light fragments for the Ag target separated for different total multiplicities of light fragments (M_L). The solid lines are two parameter fits $a\exp(-\mu Z)$ (excluding the point for $Z=12$ in $M_L=1$). The diamonds refer to the prediction of Eq. (12).

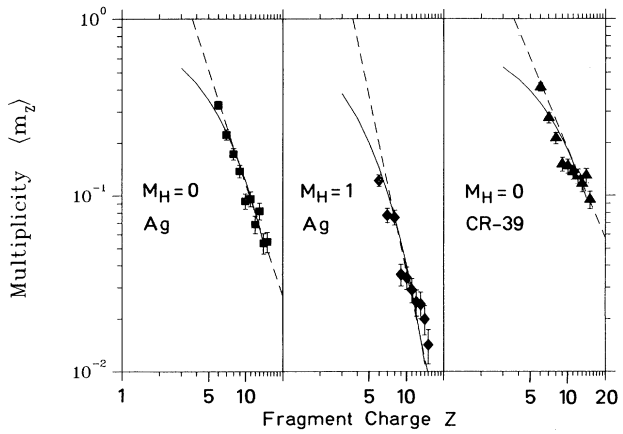

FIG. 5. Experimental mean multiplicity of light fragments for the Ag target separated in $M_H=0$ and $M_H=1$ and for the CR-39 target $M_H=0$. The solid curves are one-parameter fits $\exp(-\mu Z)$ and the dashed lines are two-parameter power-law fits.

pends on the target ($\mu=0.23\pm0.02$ for Ag and $\mu=0.17\pm0.01$ for CR-39).

The exponents μ and τ of the exponential and power-law distributions can be related to each other by requiring the two functions to be equal in value and first derivative at one value $\hat{Z}$ of Z. Equating the logarithmic derivatives leads to $\tau=\hat{Z}\mu$. If we choose the normalization point at $\hat{Z}=10$ in the middle of the interval considered, we obtain $\tau=2.3$ for the empirical value of $\mu=0.23$ for the Ag target and $\tau=1.6$ for CR-39. We want to give an argument which leads to an exponential behavior of $\langle m_Z \rangle$. It is based on the principle of minimal information (Aichelin *et al.* [28]) applied to the Poisson distributions. We define the information I of the probability distribution $P_Z(m_Z)$ by

$$I=-\sum_{Z=6}^{15}\sum_{m_Z} P_Z(m_Z)\ln P_Z(m_Z)\ , \tag{13}$$

where $P_Z(m_Z)$ is a Poissonian with mean value $\langle m_Z \rangle$.

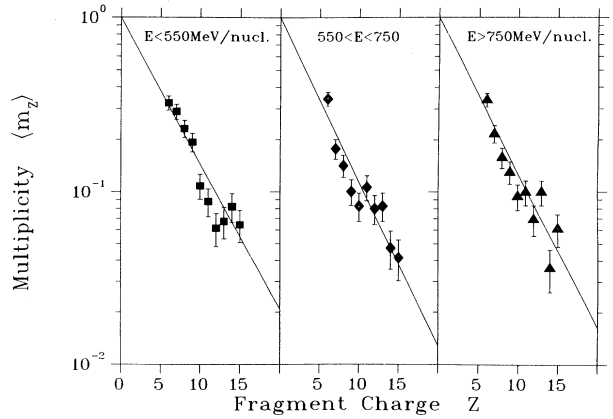

FIG. 4. Experimental mean multiplicity of light fragments for the Ag target separated in different energy bins. The solid lines are one-parameter fits $\exp(-\mu Z)$.

One obtains

$$I=\sum_{Z=6}^{15}\{\cdots\}\langle m_Z \rangle(1-\ln\langle m_Z \rangle) + \sum_{m_Z} P(m_Z)\ln(m_Z!)\ . \tag{14}$$

We neglect the last term since it is zero for $m_Z=0,1$ and of order $\langle m_Z \rangle^2/2$. Therefore the argument is restricted to small values of $\langle m_Z \rangle$. In this case Poissonian and exponential distributions are very similar. If we minimize the information under the constraint that the fragmenting system should have a certain charge (μ being the corresponding Lagrange multiplier) we require

$$\frac{\delta}{\delta\langle m_Z \rangle}\left[I-\mu\sum_{Z=6}^{15}\langle m_Z \rangle Z\right]=0\ , \tag{15}$$

which leads to

$$\langle m_Z \rangle = e^{-\mu Z}\ . \tag{16}$$

This is exactly the result of the experimental distribution. This result is interesting. It does not only lead to an exponential dependence (which is usual in these sort of arguments) but also to the coefficient 1 in front of the exponential. Despite its apparent success we are not sure how meaningful it is, i.e., to which degree dynamical effects influence the shape of the distribution.

E. Associated spallation

We have also investigated the distribution of light fragments ($6\le Z\le 15$) that are in coincidence with one heavy fragment. We call the process underlying these events associated spallation, i.e., multifragmentation associated with spallation. We introduce the probability distributions of light fragments $P_L(m_6,\ldots,m_{15})$ and $P(M_L)$ in analogy to Eqs. (2) and (3) above. The multiplicity distribution $P(M_L)$ of light fragments in spallation events is shown in Fig. 6. The values for $M_L>0$ are fitted by a

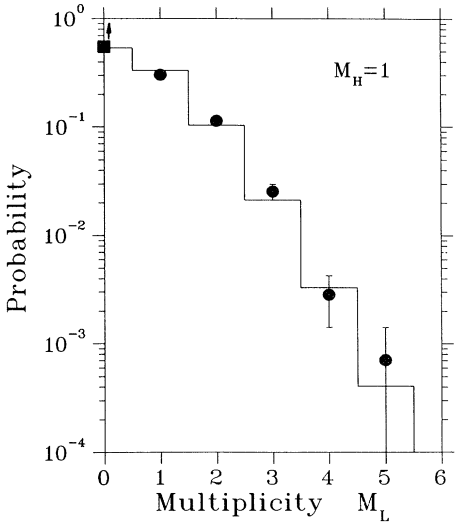

FIG. 6. Fragment multiplicity distribution for associated spallation ($M_H=1$) events of the Ag target. The data for $M_L>0$ are given by the circles, the histogram is a Poissonian fit with $\langle M_L \rangle=0.62$. The situation at $M_L=0$ is discussed in the text.

Poissionian distribution as for Fig. 1. The extrapolated value for $M_L=0$ coincides (probably accidentally) with the experimental point, though the latter one is biased by detection efficiencies (fragments with $Z \geq 65$ are only partially recorded). The missing events would contribute significantly at $M_L=0$ in Fig. 6. The correlation matrix $Q(Z_1,Z_2)$ defined in Eq. (8) is also calculated for these events. Table II shows the result. For reasons of statistics events for five values of Z have been always combined. For $Z_1<16$ and $Z_2<16$ we find the pattern already familiar from the multifragmentation events $M_H=0$: statistical independence for $Z_1 \neq Z_2$ and a Poissionian for $Z_1=Z_2$. The remaining part $Z_2>20$ of the table is also interesting: There is a positive correlation of light fragments with heavy fragments with $20 \leq Z_2 \leq 40$ and a negative one for $Z_2>40$. Thus, associated spallation occurs preferentially for medium heavy fragments.

Figure 5(b) shows the dependence of $\langle m_Z \rangle$ on Z for the associated spallation. Exponential and power-law dependences give both fair representations. We observe a steeper slope ($\mu=0.32$) as compared to $\mu=0.23$ for the $M_H=0$ events, in agreement with first findings of the detector experiments at SIS [39]. In the terminology of phase transitions introduced by Campi [40] multifragmentation events correspond to supercritical phenomena and associated spallation to critical phenomena. The functional dependence $\langle m_Z \rangle$ vs Z differs in the two event classes [Figs. 5(a) and 5(b)], but the limited range of Z values makes it impossible to identify the predicted shape change from an exponential to a power-law behavior. We come back to phase transitions in Sec. III D.

We are aware of only one other set of complete events at this energy: Waddington and Freier [3] have analyzed about 400 events recorded in an emulsion stack exposed to the 990 MeV/nucleon Au beam at the Bevalac. The target nuclei in emulsion are predominantly H, C, N, and O but also Ag and Br nuclei are present. It has not been possible to decide which target nucleus is hit in a single event. The light and heavy emulsion nuclei are similar to those contained in the CR-39 and the Ag targets, respectively. Since fission events have been removed by Waddington and Freier and the acceptance is different in both experiments a direct comparison between both sets of data is not possible. We have selected those events in which a total charge Z_{tot} between 30 and 50 is observed or would have been observed if the acceptance of the Siegen experiment is applied to the Waddington and Freier data. Under this condition the average multiplicity of fragments with charge Z measured in both experiments agrees within the error bars for $6 \leq Z \leq 30$.

III. CORRELATIONS IN FRAGMENT SIZES AND ANGLES

Multifragmentation of heavy targets has been observed at energies as low as 20 MeV/nucleon [4]. The threshold for multifragmentation is therefore much lower than the lowest beam energy ($\sim$200 MeV/nucleon) in our experiment. One may conjecture that well above threshold the beam energy dependence of multifragmentation is weak. This is not the case as a crude inspection of Fig. 7 shows.

TABLE II. The correlation matrix $Q(Z_1,Z_2)$ multiplied by 100 [Eq. (8)] binned in intervals of five charges for $M_H=1$. On the left-hand side we display the matrix, on the right-hand side the error $\sigma_Q(Z_1,Z_2)$.

	Z_1					Z_1		
	6	11	16		6	11	16	
6	7.9			6	22.4			
11	−8.0	1.7		11	15.5	97.0		
16	30.8	19.0	−2.1	16	22.2	33.1	142.5	
21	109.2	93.6	117.6	21	25.4	36.7	44.7	
Z_2 26	94.5	101.1	48.9	Z_2 26	27.3	42.5	39.7	
31	76.9	138.0	−21.7	31	27.5	51.0	29.5	
36	29.5	−2.5	−30.9	36	22.2	29.5	27.6	
41	−30.7	3.0	−36.7	41	14.2	29.2	25.2	
46	−24.1	−53.4	−47.4	46	14.8	18.5	22.5	
51	−49.1	−67.4	−91.4	51	11.5	15.1	8.6	

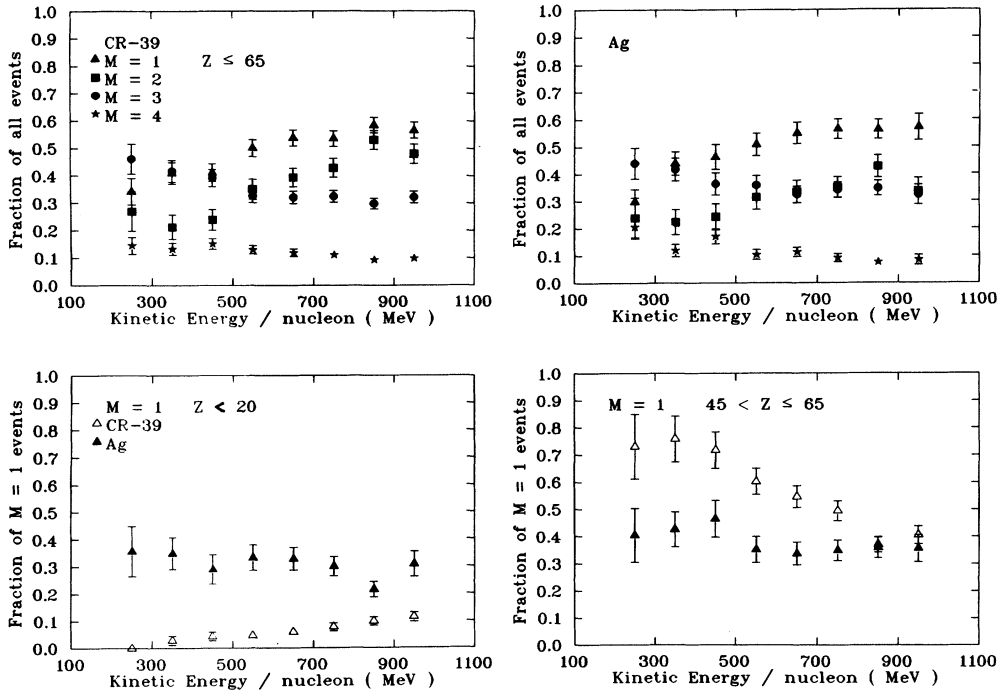

FIG. 7. Energy dependence of different processes. In the top row we display the fraction of multiplicity $f_M(\sum_M f_M = 1)$ for events with multiplicity $M=1$ to $M=4$ as a function of the beam energy and separated for both targets. The bottom row displays the fraction of ($M=1$, $6 \le Z < 20$) and of ($M=1$, $45 < Z \le 65$) events separately for both targets.

In the top row of this figure the fraction f_M, defined as the relative yield ($\sum_M f_M = 1$) of those events in which M fragments are detected, is plotted as a function of the beam energy for both targets. Above a beam energy of 500 MeV/nucleon, events in which only one fragment is detected are most frequent, while below 500 MeV/nucleon two fragment events are dominant. The relative fraction of the events with a multiplicity $M > 2$ seems to decrease with energy. This is opposite to the intuitive conjecture that with increasing energy multifragmentation events become more frequent. Less than 1% of events have a multiplicity larger than 4, though charge conservation would permit up to 13 fragments with $Z \ge 6$. This shows that at high energy and for heavy projectiles a breakup into medium ($6 \le Z \le 16$) mass fragments only, similar to the observation at low energies and for light projectiles ($\mathrm{Ne}+X \rightarrow 5\alpha + X$), does not take place. This is also in agreement with the observation in detector experiments [3] at the Bevalac that the mass distribution of the fragments in multifragmentation reactions falls off rapidly with increasing mass. Hence fragments with $Z \ge 6$ are rare.

For both targets Ag and CR-39 the events with $M=1$ become more important with increasing energy (cf. the top row of Fig. 7). The reason for this increase is different for both targets, as can be seen from the bottom figures which show the relative yield of $M=1$, $6 \le Z < 20$ and $M=1$, $45 < Z \le 65$ events. At small energies a CR-39 target is unable to "destroy" the projectile gold nucleus to such a degree that only one light fragment $20 \ge Z \ge 6$ is left over. This is a rare process even at high energies. The fraction of $M=1$ events with the fragment in $45 < Z \le 65$ is dominant ($\sim 80\%$) at low energies and decreases steadily with energy. As a consequence the number of events with $20 \le Z \le 45$ increases. Thus for CR-39 target the increase of $M=1$ events with increasing energy goes along with an increase of multifragmentation events in which the projectile nucleus is broken into many small pieces out of which only 1 is in the range between $5 \le Z \le 20$ and it goes along with an increase of spallation events where only a light remnant is observed. In the case of the silver target the fraction of events with $Z < 20$ and with $45 < Z \le 65$ stays rather constant. Thus the total increase is not due to a specific process.

We can conclude that the CR-39 target is too small in size to cause the large gold nucleus to disintegrate into small fragments (all besides one with $Z \le 5$). Independent of energy this is a rare process. The larger Ag nucleus causes more violent collisions, and it can cause complete fragmentation into clusters $Z \le 5$ and one Z with $6 \le Z \le 20$ even at low energies.

A. Associated multifragmentation, spallation, and fission events

We now proceed to investigate the events with $M=2$ and $M=3$. Events with $M > 3$ are too rare to allow for an analysis. In Figs. 8 and 9 we present a matrix of the changes measured in coincidence. The size of the box is proportional to the number of events. On the left and right sides we have the events with CR-39 and Ag targets, respectively. For the $M=2$ events we present the

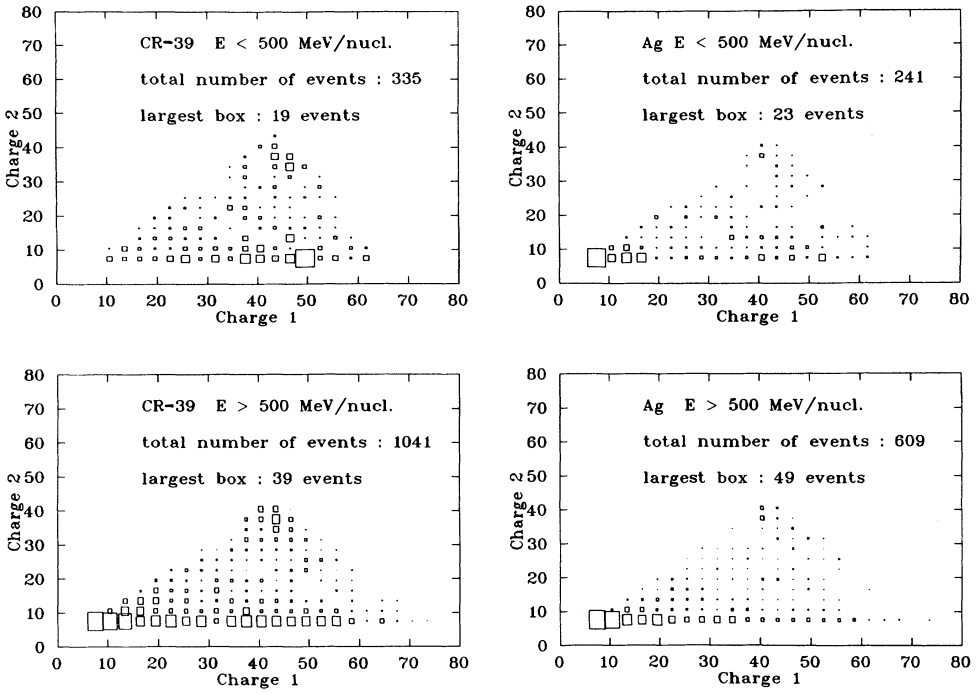

FIG. 8. Charge correlation of the multiplicity $M=2$ events separately for both targets and for two energy bins. The size of the boxes is proportional to the number of events.

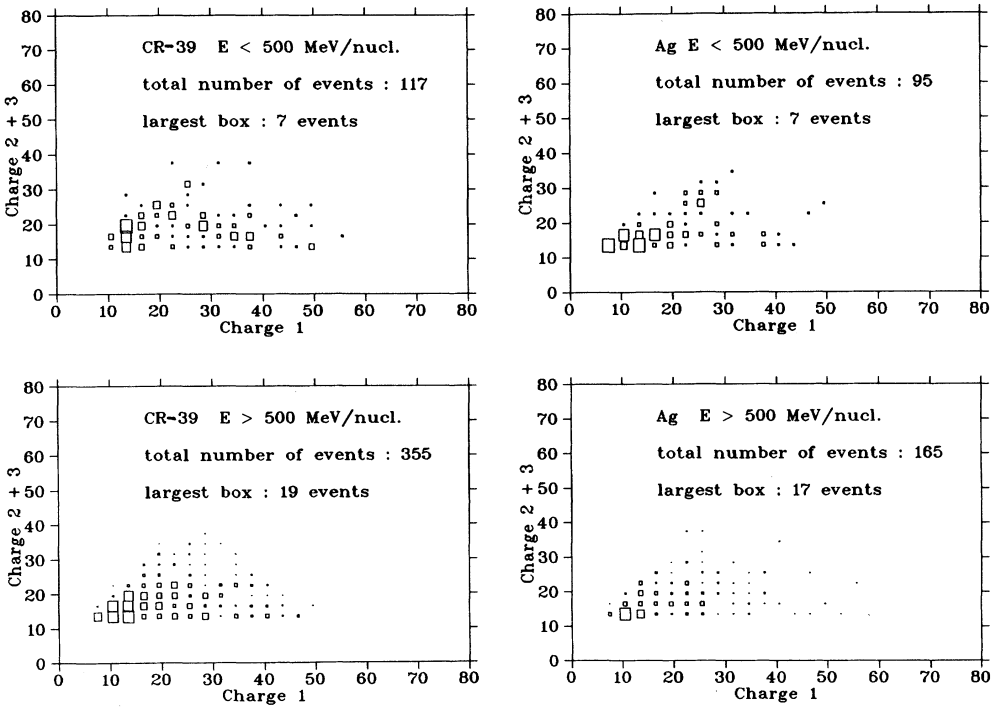

FIG. 9. Charge correlation of the multiplicity $M=3$ events separately for both targets and for two energy bins. The size of the boxes is proportional to the number of events.

matrix of both measured charges, for the $M=3$ events we display the sum of the smaller charges versus the largest charge. These correlations depend on the beam energy as well as on the target. We present therefore the data separately for both targets and separated into two energy bins ($E<500$ MeV/nucleon and $E>500$ MeV/nucleon).

1. Associated spallation

Spallation events ($M_H=1$) may have two origins: Either in peripheral reactions the small geometrical overlap of projectile and target forms a fireball which is the source of emission of singles and light fragments whereas the cold remnants gain little excitation energy by returning to a spherical shape. Or in almost central collisions the small target nucleus is stopped inside the heavy projectile followed by the equilibration of the whole system. This combined system is the source of emission of singles and light fragments. Finally, after the system has cooled down one heavy remnant is left. If at least one fragment with $Z\geq 6$ is formed, we call the process associated spallation. The present data support the second conjecture. However, for an unambiguous identification of the process a measurement of $p_{\|}$ of fragments and singles is necessary. Spallation is the dominant reaction mechanism for the interaction of the projectile with the CR-39 target. It shows a strong energy dependence (see Fig. 8). At low energies the remnant remains always large and hence the excitation energy of the emitting system is small. At high beam energies spallation events smoothly join the multifragmentation events and there is no gap in the mass yield. Spallation is also present in the $M=3$ events but only significant at low energies. However, it is not understood why events in which only light fragments are observed are contained in $M=3$ events at low energy but not in the $M=2$ events. The average mass of the largest remnant is considerably smaller for $M=3$ events as compared to the $M=2$ events. The total observed charge is roughly the same. At higher energies spallation events are virtually absent in the $M=3$ events. In reactions of the projectile with the Ag target associated spallation is a rare process. In $M=3$ events it is not seen at all, for $M=2$ we find few events which show this signature. The energy dependence seems to be weak. Both results and their difference to that with the CR-39 target are quite unexpected: Peripheral events should be similar for both targets because the slightly different curvature of the surface is unlikely to influence the process substantially. Since we see large differences for both targets we must exclude associated spallation as a peripheral process. Assuming that associated spallation is a thermal process, a similar excitation energy of the combined system should yield similar fragment distributions for both targets. The difference in the excitation energy should not be essential in view of the fact that for both targets the excitation energy is large as compared to the total binding energy.

One may therefore conjecture that central collisions are governed by geometry and not by the excitation energy.

2. Multifragmentation

Multifragmentation of the gold nucleus in reactions with the CR-39 target has an unexpectedly strong energy dependence. Below $E=500$ MeV/nucleon multifragmentation is a very rare process in the $M=2$ events. It becomes only important at higher energies. Only the $M=3$ events are mostly multifragmentation. Independent of the multiplicity the total observed charge in multifragmentation events is low, i.e., below 40. Thus multifragmentation occurs in central events where in addition many protons, α's, or small fragments are produced. A surprising observation is that multifragmentation events in CR-39 at low energies (<500 MeV/nucleon) are dominated by large multiplicities M_L. Thus it is obviously difficult to disintegrate the Au nucleus to such a degree that only one or two small fragments are left. This can hardly be attributed to insufficient excitation energy; rather, it also points towards the dominating influence of the geometry. For reactions with the silver target multifragmentation is the dominant reaction mechanism independent of the energy and of the multiplicity. The total observed charge is smaller as compared to the CR-39 target and less than half of the charge of the gold nucleus. Thus many light particles are produced in the same event.

3. Fission

We observe fission events for the reaction with the CR-39 target, but only very few for reactions with the Ag target. In view of the fact that fission is a peripheral process we do not understand this observation. One may conjecture that fission events are caused by the H nuclei contained in CR-39 in nonperipheral collisions. However, this idea contradicts the experimental observation of Warwick and Wiemann [2] who observed fission of the gold nucleus in peripheral reactions of Ne+Au. There are also almost no events where the total observed charge is between 10 and 20 units smaller than the charge of the Au nucleus. Thus fission does not occur if many small particles are simultaneously emitted, i.e., the fission fragments are always cold. Furthermore the fission fragments do not fission anymore. This would show up in the $M=3$ correlation plot.

B. Correlations between the emission angles

In this section we discuss the correlation between the emission angles in the plane perpendicular to the beam (Figs. 10 and 11) for the different processes. In Fig. 10 we display the distribution of relative angles between the two fragments for $M=2$ events. Isotropic emission would yield a constant distribution. We see that only multifragmentation events show isotropy. Spallation events favor back-to-back emission (what one expects from momentum conservation). Fission fragments peak clearly at $\Delta\phi=180°$.

The emission pattern of the $M=3$ events is displayed in Fig. 11 where the distribution of the largest relative angle between the fragments is shown. For comparison we also show the distribution expected for an isotropic

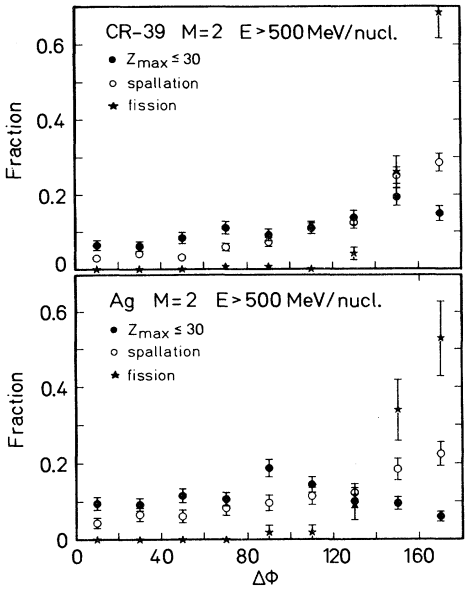

FIG. 10. Angular correlation between the fragments in $M=2$ events. We display the fraction of events as a function of the relative angle perpendicular to the beam direction for multifragmentation ($Z_{max} \leq 30$), spallation and fission events separated for both targets.

emission of the three fragments. For reactions with the CR-39 target the emission of the fragments is not random. Thus for the light target emission is not purely statistical. Emission with $\Delta\phi_{max} \approx 180°$ is favored and the emission with $220° < \Delta\phi_{max} < 360°$, i.e., where the fragments are emitted into the same hemisphere, is suppressed. One may interpret this observation as a random component superimposed by a mechanism that favors emission with $\Delta\phi_{max} \approx 180°$. This would be understandable if Coulomb forces play a more important role for the CR-39 target as compared to the Ag target. In view of the similarity of the observed charges (see Fig. 9) this could only be due to a different reaction mechanism that may be caused by geometry.

We also analyzed the angle between the major eigenvalue of the momentum tensor in the c.m. system (defined by the observed fragments) and the direction of the center of mass, but did not find any correlation. Also the energy spectra display no features that cannot be reconciled with the assumption that the relative motion of the fragments is caused by their mutual Coulomb repulsion.

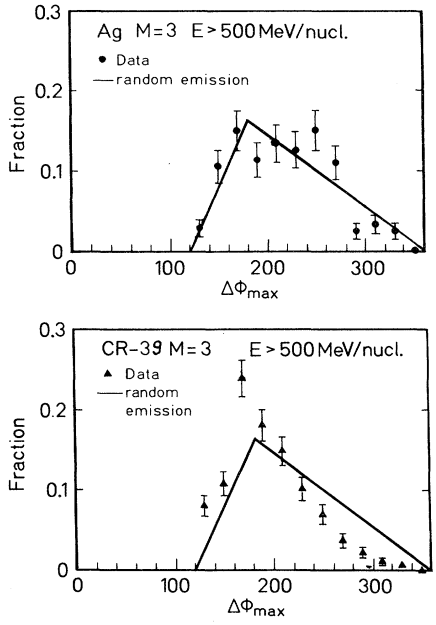

FIG. 11. Angular correlation between the fragments in $M=3$ events. We display the fraction of events as a function of the largest relative angle in the plane perpendicular to the beam direction. For comparison we display also the distribution expected from random emission.

C. Multiplicity as a function of the observed charge

We display in Fig. 12 the yield of events for a given multiplicity M as a function of total observed charge. Fission events have been excluded by requiring that the difference between both charges have to be 15 if one is around $Z_{proj}/2$. For $M=1$ events the distribution rises exponentially with increasing fragment charge (except for very large Z where the detection efficiency breaks down). This form is typically observed for spallation products. Assuming an average energy of 15 MeV/nucleon per emitted nucleon, even for $Z=40$ fragments the initial excitation energy is much less than the total available energy. This points towards more peripheral reactions.

For large Z_{tot} the events with $M>1$ are negligible. The $M=2$ events become important only if the total charge is around 60, i.e., in events in which a considerable amount of energy is transferred. One may conjecture that the process that yields one large Z, $M=2$ events is similar to $M=1$ events. If in thermal models fragments compete with α, p, and n during the evaporation of the projectile remnant, the relative ratio of $M=2$ and $M=1$ events is proportional to the emission probability

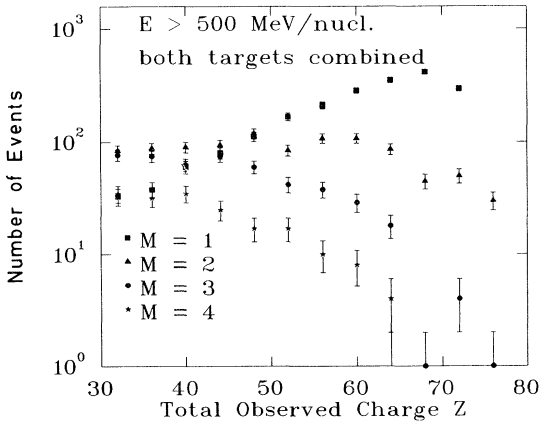

FIG. 12. Number of events as a function of the total observed charge separated for the different fragment multiplicities.

of fragments as compared to singles. At large Z_{tot} $M=2$ events are rare. This means that only at high excitation energies the probability of evaporation of fragments becomes significant. It would be interesting to see whether this energy dependence is in agreement with the standard evaporation or the microcanonical phase-space codes [16]. This tendency that high multiplicity events become rare for large Z_{tot}, continues to the $M=3$ events being only important for $Z_{tot} \lesssim 50$. Also in these events there is always one fragment much larger than the others.

D. Is there evidence for a phase transition?

Half a decade ago, Panagiotou *et al.* [12] conjectured that the form of the yield of light fragments is a direct signature for a phase transition from a liquid to a gaseous phase. Since nonthermal models like the percolation [18–21,28] of a lattice also give the same form of the mass-yield curve, the power-law dependence may be considered as a necessary but not a sufficient proof for this transition.

Nevertheless the hope of finding other observables that can be linked to the phase transition was not given up. Campi suggests [40] plotting the logarithm of the largest charge, $\ln(Z_{max})$, versus the logarithm of the second moment

$$\langle \ln S_2 \rangle = \left\langle \ln \left[\sum_{Z_i \neq Z_{max}} Z_i^2 \Big/ \sum_{Z_i \neq Z_{max}} Z_i \right] \right\rangle$$

of the remaining clusters (averaged over all events with the same Z_{max}). He studies the dependence of these observables in a percolation approach for an infinite three-dimensional lattice. He finds two branches, one for the subcritical and one for the supercritical events. Both branches meet at the point that should be populated by critical events. The predicted form of the curve $Z_{max}=f(\langle \ln S_2 \rangle)$ is also found when the events recorded by Waddington and Freier [3] are displayed. The events that fall on the critical point should then be created in a phase transition. Gross *et al.* [16] find the same curve in calculations based on a microscopic statistical model.

The present data are displayed in the variables Z_{max} vs $\ln S_2$, Fig. 13. The top row displays Z_{max} as a function of $\langle \ln S_2 \rangle$. As in the percolation of an infinite three-dimensional lattice there are two branches, the subcritical for $Z_{max} \gtrsim 50$ and the supercritical for $Z_{max} \lesssim 20$. Both branches meet at $Z_{max}=45$. The form of the curve is quite independent of whether fission events are included or excluded. Do these data present evidence for critical phenomena?

Before we start the discussion we recall that we deal with a finite system of $Z=79$. Due to charge conservation the maximal value of S_2 for a given Z_{max} is rather limited and depicted as open triangles in the upper most graph of Fig. 13. It is very instructive to plot the distribution in the $Z_{max}-S_2$ plane instead of displaying the average $\langle \ln S_2 \rangle$. This is done in the middle and the bottom figures for CR-39 and Ag targets, respectively. In both cases all possible combinations of $\ln Z_{max}$ and $\ln S_2$ occur. The curves are limited by the boundaries due to charge conservation and by the threshold $Z \geq 6$. Thus, in the nuclear case the form of the function $Z_{max}=f(\langle \ln S_2 \rangle)$ is to a large degree determined by charge conservation. We clearly see the fission fragments at $\ln Z_{max} \approx \ln S_2 \approx 3.8$, i.e., at the critical Z_{max}. We observe few events between $2.5 < \ln S_2 < 3.2$. The population of the bin $1.5 < \ln S_2 < 2.5$ is almost independent of Z_{max}.

Although one should be careful when comparing the data with the results of the calculation by Jaqaman *et al.* [17] because they refer to a proton-induced reaction ($p+$Au), it is certainly worth pointing out two important differences between our data and these calculations. First we do not observe a significant contribution of events in which one of the fission fragments fissions again. This effective three-body breakup would yield $\sum_{i=1}^{3} Z_i \approx Z_{tot}$ and should show up at $\ln S_2 \approx 2.4$, and $Z_{max} \approx 40$. Second we do not observe fission events with $Z_1+Z_2 < Z_{tot}-10$ which appear at the same value of $\ln S_2$ and slightly lower Z_{max}. Thus the experiment does not show fission-type events in reactions with large energy transfer, as already

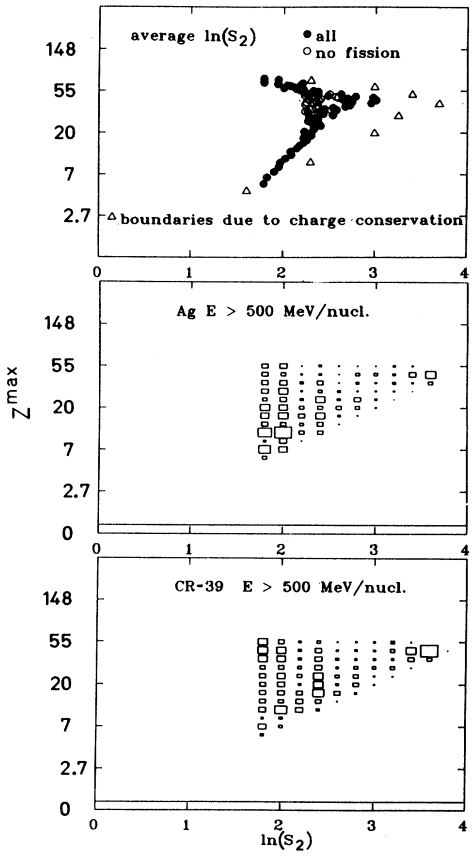

FIG. 13. The largest observed fragment Z_{max} as a function of the reduced second moment of the charges of the other observed fragments. In the top row we display the dependence of the average second moment on Z_{max} as well as the limits of the distribution due to charge conservation. The middle and bottom rows display the whole distribution for both targets. The size of the boxes corresponds to the number of events.

mentioned.

The different branches of the curve Z_{max} vs $\langle \ln S_2 \rangle$ may be associated with the phenomenological classifications of fragmentation events. The supercritical branch contains the pure multifragmentation events ($M_H=0$, $Z_{max}<20$). Spallation occurs for $Z_{max} \gtrsim 20$. In the study of multiplicity correlations we have observed events with one or several light fragments and one heavy one, predominantly for $20 \lesssim Z_{max} \lesssim 40$. This process had been termed "associated spallation." Events $Z_{max} \geq 40$ are in anticorrelation to light fragments, see Table II. The latter events lie on the subcritical branch of the curve $\ln Z_{max}$ vs $\langle \ln S_2 \rangle$. The critical zone is populated by the events termed "associated spallation."

IV. SUMMARY AND CONCLUSIONS

We have analyzed the largest set of fragment coincidence data available at present. This set contains 6610 fragmentation events of a Au projectile nucleus on a Ag or mixed target CR-39. The multiplicity distributions of light particles $6 \leq Z \leq 15$ show a Poissonian behavior. For the Ag target the angular correlation (in the plane perpendicular to the beam direction) is in agreement with random emission. These two results favor the interpretation that multifragmentation is a statistical process, at least for the Ag target. The shape of the mean multiplicity $\langle m_Z \rangle$ vs Z is compatible with an exponential or a power law. If one uses an exponential shape, $\langle m_Z \rangle = a \exp(-\mu Z)$, one finds $a=1$.

A number of correlations of fragment sizes and their energy dependences have been established. It is not possible to cast them into simple quantitative relations. They are displayed in figures; many observations remain unexplained. We find unexpectedly strong energy dependences. The differences for the two targets, Ag and CR-39 are sizable. However, one should be careful with the results of CR-39, since it is a mixed target. It is for this reason that we have limited the quantitative analysis in Sec. II to the Ag target only.

We have looked into the question of a liquid-gas phase transition. If it is present at all, it is expected to be washed out considerably since we deal with a finite system. The relation Z_{max} vs $\langle \ln S_2 \rangle$ proposed by Campi has been seen in the data, but we argue that it is mainly determined by charge conservation. We see a continuous transition from the supercritical branch (multifragmentation) into the "critical" region (associated spallation) and out on the subcritical branch (spallation with very few light fragments) (see Figs 8 and 9). Although the mean multiplicity $\langle m_Z \rangle$ of light particles does indeed display some changes in the shape when going into the region of "critical" events, we are not able to identify them as positive signs for a phase transition.

ACKNOWLEDGMENTS

This work was supported in part by the Gesellschaft für Schwerionenforschung (GSI) Darmstadt under Contract No. HD HU T and the German Bundesminister für Forschung und Technologie (BMFT) under Contract No. 06 Si 146. C.L. was supported by CNPq, Brazil, and A.A.-M. by the Internationales Büro, Jülich.

[1] J. Hüfner, Phys. Rep. **125**, 129 (1985).
[2] A. I. Warwick *et al.*, Phys. Rev. C **27**, 1083 (1983).
[3] C. J. Waddington and P. S. Freier, Phys. Rev. C **31**, 888 (1985).
[4] B. Jakobsson *et al.*, Nucl. Phys. **A509**, 195 (1990); Z. Phys. A **307**, 293 (1977); Phys. Scr. **38**, 132 (1988); Nucl. Phys. **A488**, 251c (1988).
[5] Y. D. Kim *et al.*, Phys. Rev. Lett. **63**, 494 (1989).
[6] D. J. Fields *et al.*, Phys. Rev. C **34**, 536 (1986).
[7] R. Trockel *et al.*, Phys. Rev. C **39**, 729 (1989).
[8] H. H. Gutbrod *et al.*, Rep. Prog. Phys. **52**, 1267 (1989).
[9] K. G. R. Doss, Phys. Rev. Lett. **89**, 2720 (1987).
[10] J. W. Harris, Nucl. Phys. **A471**, 241c (1987).
[11] M. E. Fisher, Physics **3**, 255 (1967).
[12] A. D. Panagiotou *et al.*, Phys. Rev. Lett. **52**, 496 (1984).
[13] J. Hüfner and D. Mukhopadhyay, Phys. Lett. **173B**, 373 (1986).
[14] S. E. Koonin and J. Randrup, Nucl. Phys. **A356**, 223 (1981); **A474**, 173 (1987).
[15] J. P. Bondorf, R. Donangelo, I. N. Mishustin, C. J. Pethick, H. Schulz, and K. Sneppen, Nucl. Phys. **A443**, 321 (1985); J. P. Bondorf, R. Donangelo, I. N. Mishustin, and H. Schulz, *ibid.* **A444**, 460 (1985).
[16] Sa Ban-hao and D. H. E. Gross, Nucl. Phys. **A437**, 643 (1985); X. Z. Zhang, D. H. E. Gross, and Y. M. Zheng, *ibid.* **A461**, 641 (1987); **A461**, 668 (1987).
[17] H. R. Jaqaman, G. Papp, and D. H. E. Gross, Nucl. Phys. **A514**, 327 (1990).
[18] W. A. Friedman and W. G. Lynch, Phys. Rev. C **28**, 16 (1983).
[19] C. Barbagallo, J. Richert, and P. Wagner, Z. Phys. A **324**, 97 (1986).
[20] R. J. Charity *et al.*, Nucl. Phys. **A483**, 371 (1988).
[21] J. A. Lopez and J. Randrup, Nucl. Phys. **A491**, 477 (1989); **A503**, 183 (1989); **A512**, 345 (1989).
[22] J. Nemeth *et al.*, Z. Phys. A **325**, 347 (1986).
[23] W. Bauer *et al.*, Nucl. Phys. **A452**, 699 (1986).
[24] J. Desbois, Nucl. Phys. **A466**, 724 (1987).
[25] W. Bauer, Phys. Rev. C **38**, 1297 (1988).
[26] C. O. Dorso *et al.*, Phys. Lett. B **244**, 165 (1990).
[27] J. Aichelin, J. Hüfner, and R. Ibarra, Phys. Rev. C **30**, 107 (1984).
[28] J. Aichelin and J. Hüfner, Phys. Lett. **136B**, 15 (1984).
[29] J. Aichelin, Phys. Rev. C **30**, 718 (1984).
[30] J. Aichelin *et al.*, Phys. Rev. C **37**, 2451 (1988).
[31] G. Peilert *et al.*, Phys. Rev. C **39**, 1402 (1989).
[32] A. Bohnet, Phys. Rev. C (in press).
[33] J. Aichelin, Phys. Rep. (in press).
[34] D. Boal *et al.*, Phys. Rev. C **40**, 601 (1989), and references therein.
[35] S. M. Kiselev, Phys. Lett. B **240**, 23 (1990).
[36] K. K. Gudima *et al.*, Phys. Lett. B **234**, 1 (1990).
[37] S. Leray *et al.*, Nucl. Phys. **A511**, 414 (1990).
[38] J. Dreute *et al.*, Phys. Rev. C **44**, 1058 (1990), the preceding paper.
[39] P. Kienle, GSI Report No. 90-43, 1990.
[40] X. Campi, Phys. Lett. B **208**, 351 (1988).